

# Intramolecular Energy Transfer in Compounds with Two 1-Pyrenoate Groups Separated by Methylene Spacers

Julio Bravo,<sup>1</sup> Francisco Mendicuti,<sup>2</sup> Enrique Saiz,<sup>2</sup> and Wayne L. Mattice<sup>3</sup>

Received January 20, 1995; accepted December 14, 1995

Steady-state fluorescence anisotropy ( $r$ ) and fluorescence lifetime ( $\tau$ ) measurements have been used to study the efficiency of nonradiative singlet energy transfer as a function of alkane size in 1-pyrenecarboxylic acid alkanediyl esters (as a function of  $m$  in  $\text{Py-COO-(CH}_2\text{)}_m\text{-OOC-Py}$ , where Py denotes pyrene substituted in the 1-position, and  $m = 2-6$ ). Experiments were performed in media of different viscosity,  $\eta$ , obtained by changing the temperature (from  $-20$  to  $40^\circ\text{C}$ ) of dilute solutions in ethylene glycol and by examination of the compounds in a solid matrix of poly(methyl methacrylate) (PMMA) at ambient temperature. The  $\text{Py-COO-(CH}_2\text{)}_m\text{-OOC-Py}$  exhibit intramolecular excimer emission in ethylene glycol at these temperatures, but the intensity of this emission is much lower than when these compounds are placed in common solvents of lower  $\eta$ . The values of  $\tau$  indicate that excitation hopping or intramolecular energy transfer takes place between the chromophores attached to the ends of the alkane bridges. Values of  $r$  obtained by the extrapolations  $T/\eta \rightarrow 0$  or  $\tau T/\eta \rightarrow 0$  in ethylene glycol, as well as the values obtained in the rigid matrix of PMMA, show very little dependence on  $m$ . A theoretical conformational analysis, using the rotational isomeric state (RIS) model, was also performed. The combination of the experimental results for  $r$  in the media of high  $\eta$  with the theoretical (RIS) analysis produces an estimated value of  $21 \pm 2 \text{ \AA}$  for the Förster radius in  $\text{Py-COO-(CH}_2\text{)}_m\text{-OOC-Py}$ .

**KEY WORDS:** Intramolecular energy transfer; 1-pyrenoate; methylene spacers; fluorescence anisotropy; fluorescence lifetime.

## INTRODUCTION

Pyrene can form excimers that are of inter- or intramolecular origin. The prototype of the former situation is demonstrated in the study of free pyrene itself in solutions of varying concentration.<sup>(1)</sup> Simple examples of the latter situation are presented by molecules that are constructed with two pyrenes connected by a hydrocarbon spacer, as in 1,3-dipyrenylpropane,<sup>(2-4)</sup> the isomeric 2,4-dipyrenylpentanes,<sup>(3,5-8)</sup> and  $\alpha,\omega$ -dipyrenylalkanes.<sup>(8,9)</sup> Oxygen at-

oms can be introduced into the spacer as ethers,<sup>(3,5,10)</sup> esters,<sup>(11,12)</sup> or a combination of ethers and esters.<sup>(13)</sup>

The characteristic distance for the interaction of the two chromophores that form the excimer is  $3-4 \text{ \AA}$ .<sup>(14)</sup> Pyrene-pyrene interaction can also occur over larger distances via nonradiative singlet energy transfer (Förster transfer). For free pyrene, the Förster radius ( $R_0$ ) for this process is  $10.05 \text{ \AA}$ .<sup>(15)</sup> Since the fluorescence quantum yield ( $\phi$ ) and overlap integral ( $J$ ), which are involved in establishing the value of  $R_0$ , are sensitive to the presence of substituents directly bonded to the pyrene, a different value of  $R_0$  may be found when pyrene is not free but is, instead, incorporated into a larger molecule by covalent bonds.

Here we study the fluorescence anisotropy ( $r$ ) and efficiency of intramolecular nonradiative singlet energy

<sup>1</sup> Departamento de Ingeniería Industrial, Universidad Carlos III de Madrid, 28911 Leganés, Spain.

<sup>2</sup> Departamento de Química Física, Universidad de Alcalá, Alcalá de Henares, Madrid, Spain.

<sup>3</sup> Institute of Polymer Science, The University of Akron, Akron, Ohio 44325-3909.

transfer ( $\Phi$ ) between two pyrenes bonded via ester groups to spacers constructed from two to six methylene groups. These 1-pyrenecarboxylic acid alkanediyl esters have the structure  $\text{Py-COO-(CH}_2)_m\text{-OOC-Py}$ , where Py denotes pyrene substituted in the 1-position. The dependence of  $r$  and  $\Phi$  on  $m$  is different from the dependence of the extent of excimer formation, as measured by  $I_D/I_M$ , where  $I_D$  and  $I_M$  denote the intensities of excimer (dimer) and monomer emission, respectively.<sup>(12)</sup> This result from the experiments is rationalized with an analysis of the conformations of the compounds. The value of  $R_0$  for self-transfer by the Py in these compounds is twice as large as the value of  $R_0$  for self-transfer by free pyrene.

## EXPERIMENTAL

The diesters with the structure  $\text{Py-COO-(CH}_2)_m\text{-OOC-Py}$  are abbreviated Py#MPy. The number of methylene groups,  $m$ , is substituted for # to denote a particular member of this series of compounds. They were synthesized and purified as described previously.<sup>(12)</sup> In brief, the diesters were obtained by reaction of 1-pyrenoyl chloride with  $\text{HO-(CH}_2)_m\text{-OH}$  in chloroform, in the presence of triethylamine. For the model compound with a single chromophore, the methyl ester of 1-pyrenic acid (methyl 1-pyrenecarboxylate; PyM), the glycol was replaced with methanol. Samples in poly(methyl methacrylate) (PMMA) were prepared in the same manner described previously,<sup>(16)</sup> starting from solutions of the compounds in methyl methacrylate that had an optical density around 0.2 at the wavelength used for excitation (340 nm).

Methyl methacrylate (Merck; >99%, stabilized with hydroquinone) and methanol (Fisher; reagent grade) were distilled before use. The other solvents used (ethyleneglycol, 1,2-dichloroethane, and *p*-dioxane) were spectrophotometric grade from Aldrich, and they were used without further purification.

All steady-state measurements were performed with an SLM Aminco 8100 spectrofluorimeter equipped with a cooled photomultiplier and double and single monochromators in the excitation and emission paths, respectively. Slits in most of the experiments were fixed at 2 and 4 nm for excitation and emission, respectively. Corrected emission or excitation spectra were obtained with the excitation polarizer oriented in the vertical position and the emission polarizer oriented 54.7° from vertical.<sup>(17)</sup> Right-angle geometry for measurements in solution and front-face illumination (at 30°) for measurement of vitrified glass samples were used. Typical absorb-

ances at the wavelength of excitation for samples in solution were about 0.1 for steady-state and time-resolved fluorescence.

Anisotropy measurements were performed for the compounds in media of different viscosity,  $\eta$ , by using ethylene glycol as solvent and changing the temperature from -20 to 40°C and by measurements in which the compounds are dispersed in a solid matrix of PMMA. The anisotropy of the fluorescence was measured by the "L" method, as described by Lakowicz.<sup>(18)</sup>

$$r = \frac{I_{VV} - GI_{VH}}{I_{VV} + 2GI_{VH}} \quad (1)$$

where  $I_{VV}$  and  $I_{VH}$  are, respectively, the intensities of the emission when both polarizers are vertical and when the excitation polarizer is vertical and the emission polarizer is horizontal, and  $G = I_{HV}/I_{HH}$  corrects for any cause of depolarization in the optical system. The polarizers in the excitation and emission path are horizontal and vertical respectively, for measurements of  $I_{HV}$  and they are both horizontal for  $I_{HH}$ .

Fluorescence decays were obtained by time-resolved fluorimetry using the single-photon counting technique on a modified PRA fluorimeter. An Edinburgh Instruments nF9000 flash lamp was employed as the light source, using  $\text{N}_2$  as the gas. The optimum conditions found were 1.5 atm, 30 kHz, 6 kV, and 0.3 mm as the electrode gap. With these conditions the typical half-width of the lamp pulse was 1.8 ns. Deconvolution taking into account the lamp pulse shape was performed. Fluorescence decays for all samples were measured in aerated solutions in ethylene glycol at three temperatures (-15, 15, and 40°C) at the monomer emission band (408 nm) upon excitation at 340 nm. The quality of the fits was judged by the values of the reduced  $\chi^2$  and the distribution of the residuals.

## RESULTS

### Steady-State Fluorescence

Figures 1 and 2 depict the corrected emission spectra at different wavelengths for PyM and Py5MPy in methanol at 25°C. Solvent blanks were subtracted from the emission spectra. Emission (and excitation) spectra do not change significantly upon selection of different excitation (or emission) wavelengths. Figures 3 and 4 depict corrected emission spectra for PyM and Py#MPy in ethylene glycol at -15 and 35°C, respectively, upon excitation at 340 nm. As previously,<sup>(12)</sup> bands shifted to

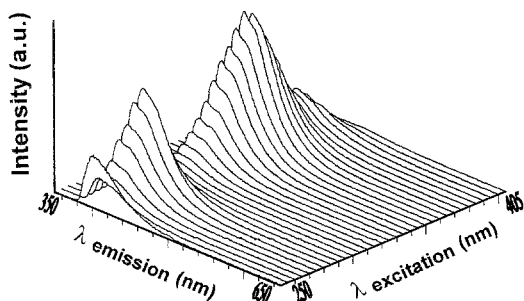


Fig. 1. Corrected emission spectra obtained at different excitation wavelengths (in the range 205–405 nm) for PyM in methanol at 25°C.

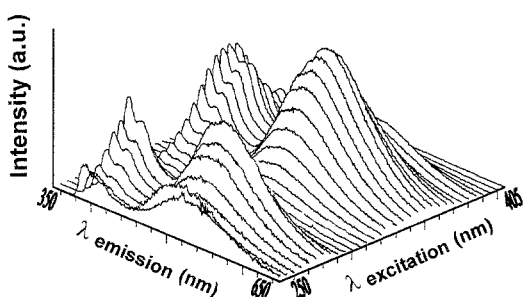


Fig. 2. Corrected emission spectra obtained at different excitation wavelengths (in the range 205–405 nm) for Py5MPy in methanol at 25°C.

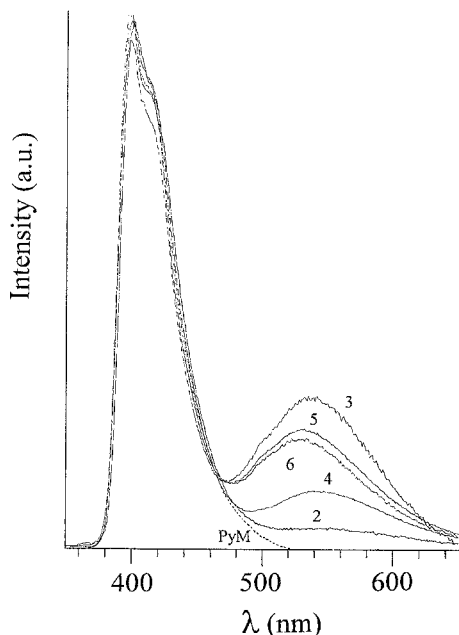


Fig. 3. Corrected emission spectra for PyM and Py#MPy in ethylene glycol at  $-15^{\circ}\text{C}$ . The unnumbered spectrum is PyM, and the integers on the remaining spectra are the values of # in Py#MPy.

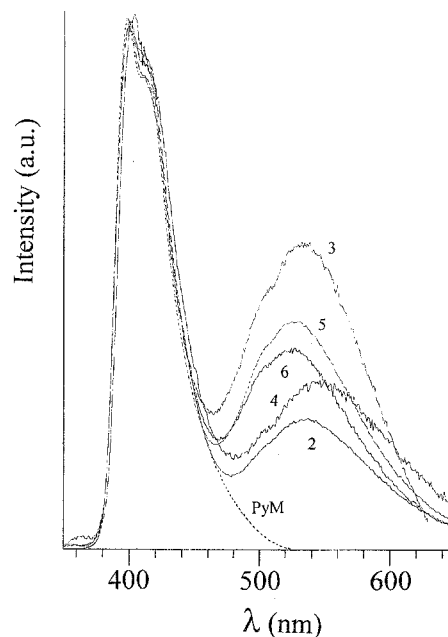


Fig. 4. Corrected emission spectra for PyM and Py#MPy in ethylene glycol at  $35^{\circ}\text{C}$ . The unnumbered spectrum is PyM, and the integers on the remaining spectra are the values of # in Py#MPy.

the red from the monomer band of PyM were attributed to intramolecular excimer formation which depends strongly on the  $m$  and  $\eta$  of the solvent. The amount of intramolecular excimer shown in Figs. 3 and 4 is smaller than when the compounds are dissolved in common solvents of much lower  $\eta$ .

Energy migration is an intrinsic cause of depolarization of fluorescence, but the depolarization can also be caused by extrinsic mechanisms which produce rotational diffusion of the fluorophore, by segmental motion and/or rotational diffusion of the whole molecule. These extrinsic causes of depolarization depend on  $\eta$  and on  $\tau$ . For a spherical molecule with a decay described by a single exponential, the Perrin equation relates  $r$ ,  $\eta$ , and  $\tau$  as<sup>(14,19,20)</sup>

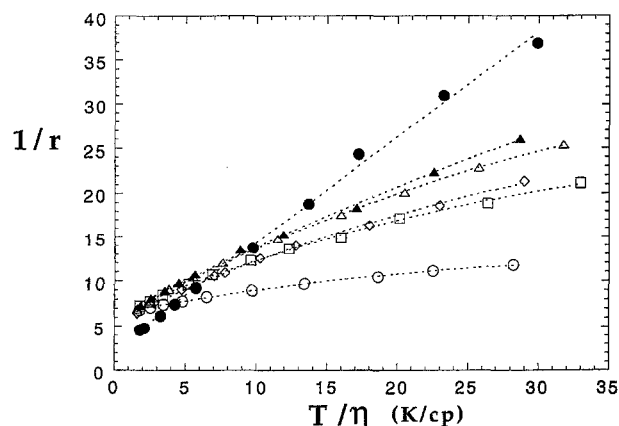
$$\frac{1}{r} = \frac{1}{r_0} \left( 1 + \frac{k\tau T}{V\eta} \right) \quad (2)$$

where  $r_0$  is the anisotropy in a rigid medium,  $V$  is the volume of the particle,  $T$  is the absolute temperature, and  $k$  is Boltzman's constant.

Table I collects the values of  $r$  for PyM and Py#MPy in PMMA for two excitation and emission slits bandpass sets (2/2 and 2/4 nm) and for two sets of excitation and emission wavelengths. The largest values of  $r$  are always obtained for PyM, and they are close to 0.4, as expected for a random orientation of independent

**Table I.** Anisotropies for PyM and Py#MPy in PMMA at the Excitation/Emission Wavelengths Shown

Compound	340/408 <sup>a</sup>	340/436 <sup>a</sup>	340/408 <sup>b</sup>	340/436 <sup>b</sup>
PyM	0.404	0.343	0.406	0.345
Py2MPy	0.213	0.192	0.216	0.192
Py3MPy	0.217	0.206	0.216	0.205
Py4MPy	0.211	0.187	0.220	0.197
Py5MPy	0.222	0.209	0.226	0.213
Py6MPy	0.212	0.186	0.211	0.187

<sup>a</sup> Excitation and emission slits of 2 nm.<sup>b</sup> Excitation and emission slits of 2 and 4 nm, respectively.**Fig. 5.** Representation of  $1/r$  vs  $T/\eta$  for PyM and Py#MPy in ethylene glycol over the temperature range  $-20$  to  $40^\circ\text{C}$ . (●) PyM, (○) 2, (□) 3, (◇) 4, (△) 5, and (▲) 6.**Table II.** Values of  $r_0$  and  $[d(1/r)/d(T/\eta)]_{T/\eta \rightarrow 0}$  for PyM and Py#MPy in Ethylene Glycol

Compound	$r_0$	$[d(1/r)/d(T/\eta)]_{T/\eta \rightarrow 0}$ ( $10^{-3}$ kg/kms)
PyM	0.405	1.193
Py2MPy	0.155	0.288
Py3MPy	0.161	0.674
Py4MPy	0.181	0.744
Py5MPy	0.175	0.874
Py6MPy	0.166	0.833

chromophores in a rigid medium. Values of  $r$  for Py#MPy are smaller than 0.4, and they do not show any appreciable dependence on  $m$ . Average values of  $r$  for Py#MPy are  $0.217 \pm 0.007$  and  $0.197 \pm 0.014$ , as measured at 340/408 and 340/436 nm, respectively.

Figure 5 depicts  $1/r$  vs  $T/\eta$  for PyM and Py#MPy when the changes in  $T/\eta$  are produced by changing  $T$  over the  $60^\circ$  range— $20$  to  $40^\circ$  with ethylene glycol as the solvent. The data for PyM give a linear fit, but the

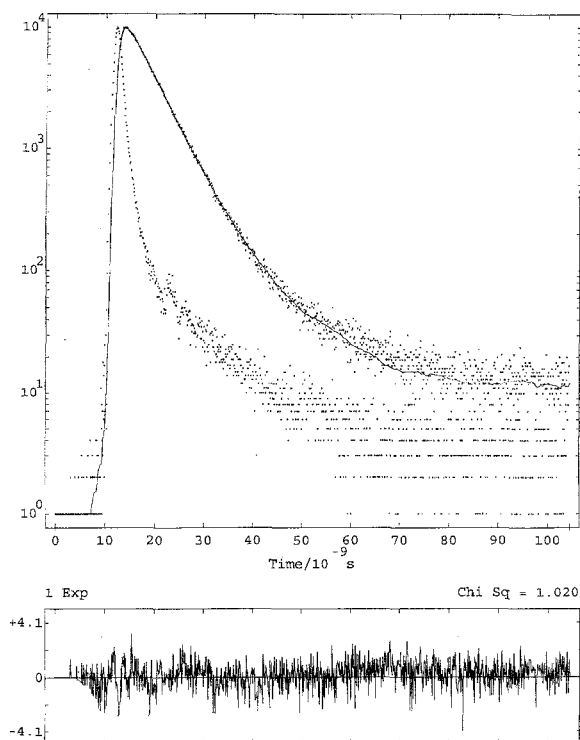
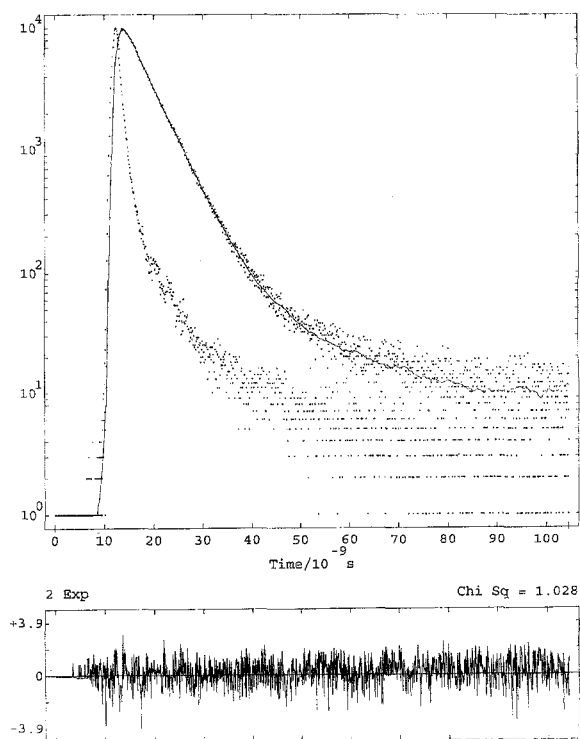
**Fig. 6.** Fluorescence decay, reduced  $\chi^2$ , and the distribution of the residuals for PyM in ethylene glycol at  $-15^\circ\text{C}$ .**Fig. 7.** Fluorescence decay, reduced  $\chi^2$ , and the distribution of the residuals for Py3MPy in ethylene glycol at  $-15^\circ\text{C}$ .

Table III. Decay Parameters for PyM and Py#MPy in Ethylene Glycol

$T(^{\circ}\text{C})$	Property	PyM	Py2MPy	Py3MPy	Py4MPy	Py5MPy	Py6MPy
-15	$\tau_1$ (ns)	4.8	3.6	3.9	4.8	4.8	5.0
	$\tau_2$ (ns)	—	1.6	5.4	31.6	25.1	24.0
	$w_1^a$	1	0.73	0.65	0.95	0.98	0.97
	$\chi^2$	1.02	1.16	1.04	1.03	1.14	1.10
15	$\tau_1$ (ns)	4.9	1.6	3.6	4.3	4.6	4.6
	$\tau_2$ (ns)	—	3.9	7.7	22.9	27.3	16.1
	$w_1^a$	1	0.84	0.93	0.96	0.99	0.97
	$\chi^2$	1.26	1.32	1.03	1.01	1.01	1.20
40	$\tau_1$ (ns)	4.9	1.1	2.6	3.2	3.7	3.7
	$\tau_2$ (ns)	—	4.7	4.7	9.7	21.5	20.6
	$w_1^a$	1	0.91	0.89	0.92	0.99	0.99
	$\chi^2$	1.31	1.46	1.09	1.07	1.03	1.02

$$^a w_1 = 1 - w_2 = \alpha_1 \tau_1 (\alpha_1 \tau_1 + \alpha_2 \tau_2)^{-1}.$$

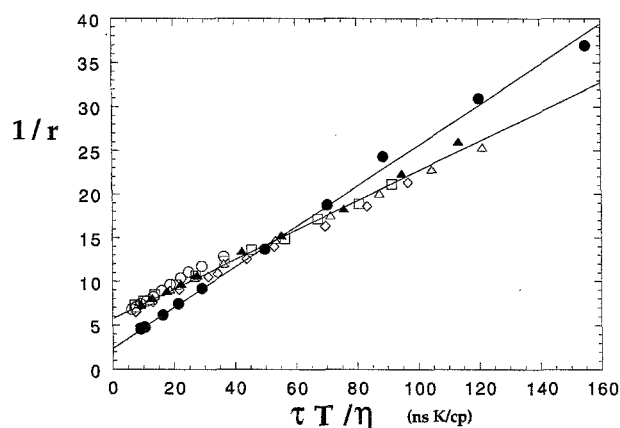


Fig. 8. Representation of  $1/r$  vs  $T/\eta$  for PyM and Py#MPy in ethylene glycol over the temperature range  $-20$  to  $40^{\circ}\text{C}$ . (●) PyM, (○) 2, (□) 3, (◇) 4, (△) 5, and (▲) 6.

description of the data for each Py#MPy requires a second-order polynomial instead. As  $T$  increases and  $\eta$  decreases, the fluorescence anisotropy decreases ( $1/r$  increases), due to a higher segmental mobility and/or faster rotational diffusion of the molecule, or to a greater efficiency of energy transfer. The increase in energy transfer can result from the relative diffusion of both chromophores from larger to smaller separations, where the transfer is more probable.<sup>(21)</sup>

Table II collects values of  $r_0$  obtained from the intercepts and initial slopes at  $T/\eta \rightarrow 0$  from plots such as Fig. 5. The highest slope is obtained for PyM, probably because of the faster rotational diffusion of a single pyrene group, compared to the two groups in Py#MPy. For the bichromophoric compounds, the slope increases significantly as  $m$  increases. These results could be due to an increase in motion of the chromophore bonded to

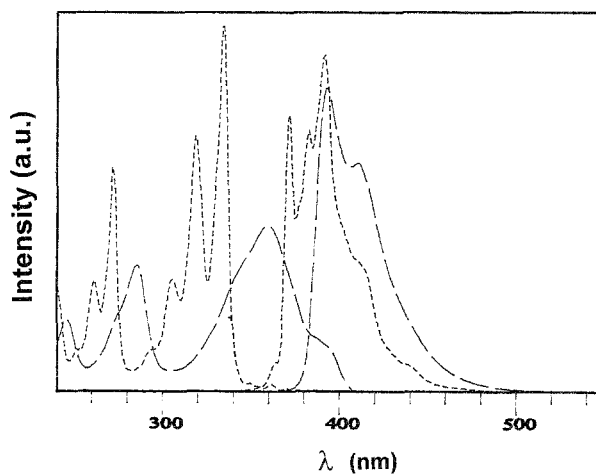


Fig. 9. Excitation and emission spectra, normalized to one, for pyrene (—) and PyM (---) in *p*-dioxane at  $25^{\circ}\text{C}$ . Excitation was at  $340$  nm for the emission spectra, and emission was monitored at  $408$  nm for the excitation spectra.

a more flexible chain at larger  $m$ . At lower  $\eta$  this effect is trivial. Extrapolation of  $1/r$  to  $T/\eta \rightarrow 0$  yields a value of  $r_0$  for PyM that is close to  $0.4$ . Similar extrapolations for Py#MPy do not show any monotonic dependence of  $r_0$  on  $m$ . From the extrapolated values of  $1/r$  for Py#MPy, an average for  $r_0$  of  $0.168 \pm 0.013$  was obtained.

### Fluorescence Lifetimes

Figures 6 and 7 depict examples of the decays for the fluorescence of PyM and Py3MPy in ethylene glycol at  $-15^{\circ}\text{C}$ . The decay of the fluorescence from PyM was fitted to a single exponential,

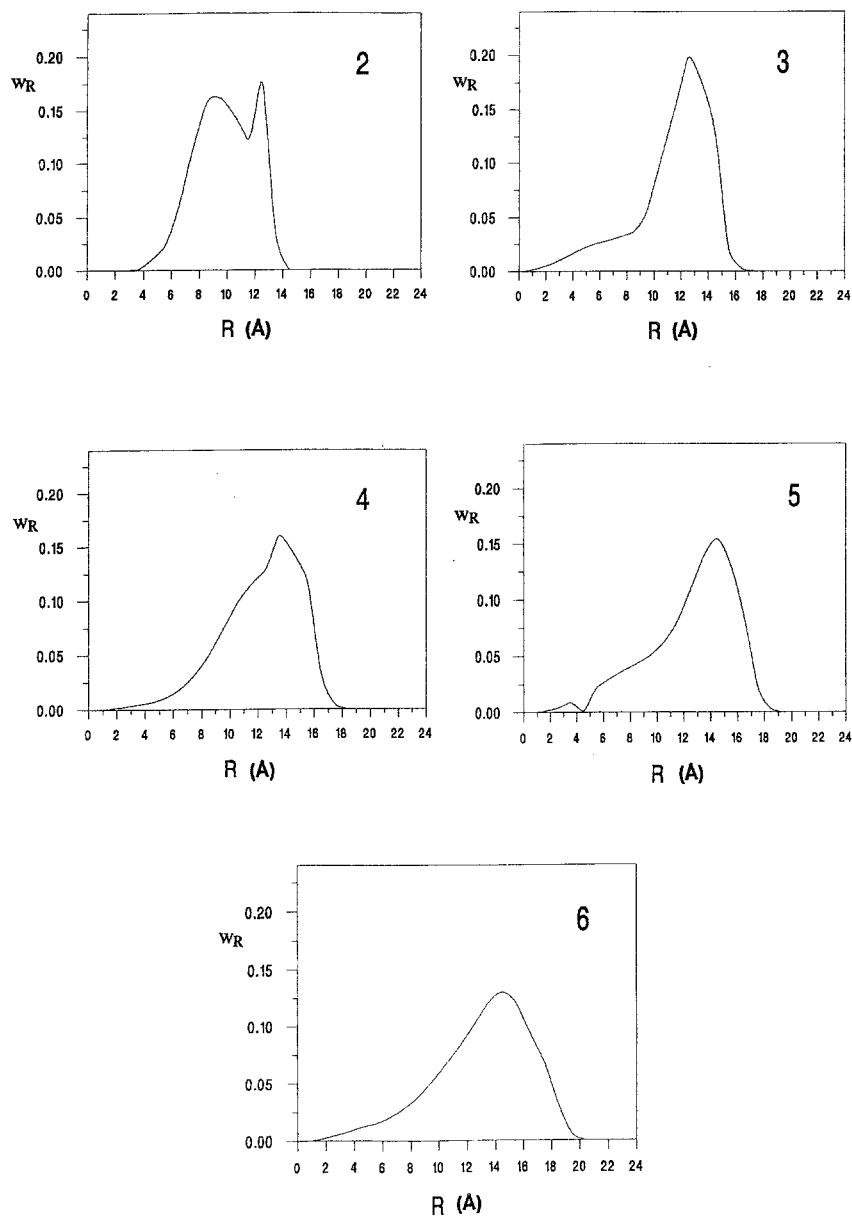


Fig. 10. Distribution function,  $w_R$ , for the distance between centers of the pyrene rings for Py#MPy with the indicated value of  $m$ .

$$I(t) = \alpha \exp(-t/\tau) \quad (3)$$

and a sum of two exponentials was used for fitting the decay of the fluorescence from Py#MPy,

$$I(t) = \alpha_1 \exp(-t/\tau_1) + \alpha_2 \exp(-t/\tau_2) \quad (4)$$

The results are reported in Table III. The fluorescence lifetime for the model compound containing a single chromophore, PyM, has a value of 4.8–4.9 ns, and it does not depend significantly on  $T$  (and  $\eta$ ). The term from Eq. (4) that makes the dominant contribution to the

fluorescence for Py#MPy gives a monomer fluorescence lifetime in these bichromophoric compounds that depends on  $T$  at each value of  $m$ . As  $T$  increases (or  $\eta$  decreases), the monomer fluorescence lifetime for Py#MPy decreases.

There are several processes that might account for the fact that a change in  $\eta$  affects  $\tau$  in Py#MPy but does not affect  $\tau$  in PyM. Relative diffusion of the two chromophores in Py#MPy to distances (or orientations) more conducive to energy transfer during the lifetime of the excited state of the monomer would produce a more

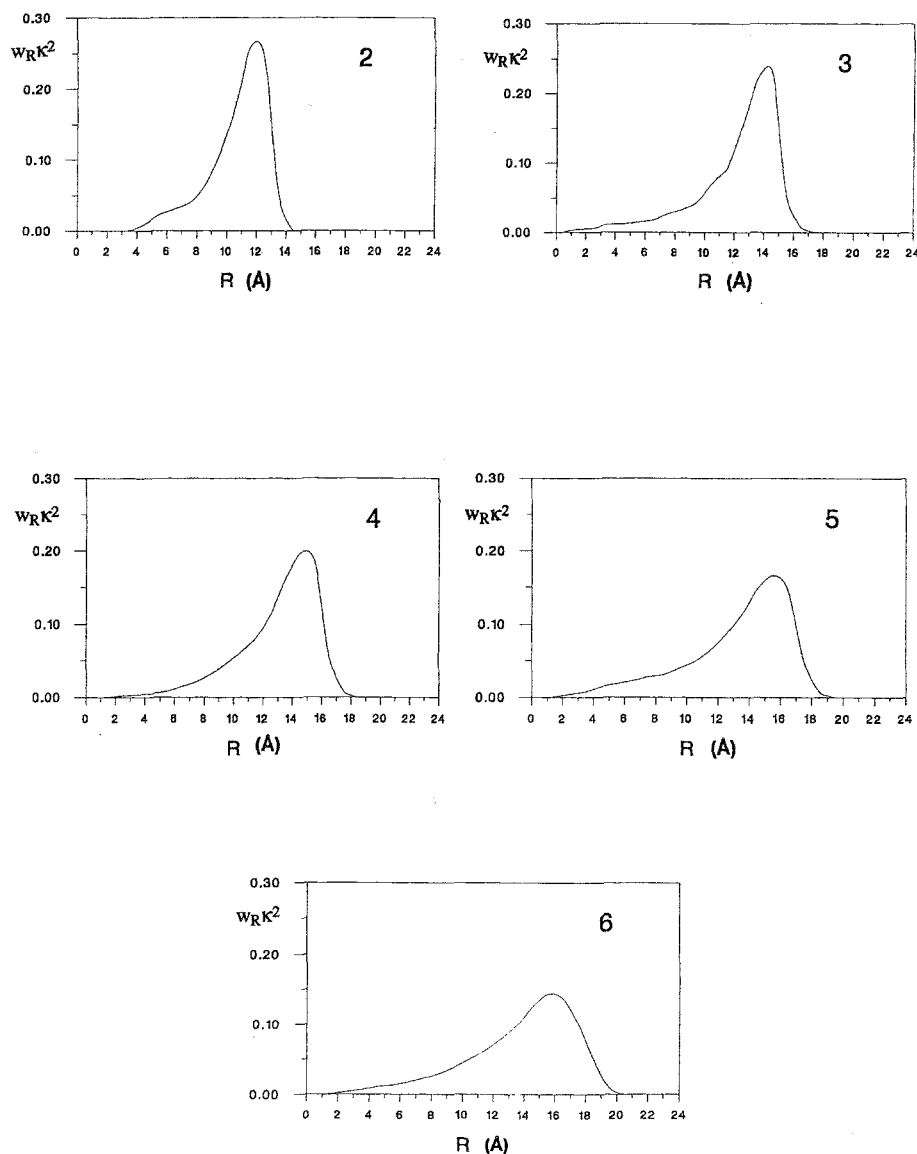


Fig. 11. Distribution of  $w_R k^2$  for Py#MPy at the indicated value of  $m$ .

rapid decay of donor fluorescence.<sup>(21)</sup> This effect could also arise from increased thermal deactivation of the electronic excited state of pyrene in the Py#MPy due to an increase in  $T$  or decrease in  $\eta$  (J. E. Guillet and Y. Li, personal communication, July 1994). This observation is in agreement with the increase in the fluorescence lifetime, at a particular  $T$  or  $\eta$ , as  $m$  increases. However, these explanations cannot be applied to PyM, where the lifetime is independent of  $T$  and  $\eta$ . Perhaps the qualitative difference in the behavior of PyM and the Py#MPy can be attributed to the influence of segmental motion of the fluorophores in Py#MPy, which is much

more rapid than the rotational diffusion of the molecule as a whole.

The fluorescence lifetimes for each compound can be incorporated into the analysis of  $r$ , as shown by Eq. (2). Figure 8 depicts  $1/r$  vs  $\tau T/\eta$ . Linear plots are obtained for each Py#MPy, in contrast to the curvature observed in  $1/r$  vs  $T/\eta$  in Fig. 5. All points for the Py#MPy can be fitted to the same linear equation, which gives a value of  $r_0 = 0.174 \pm 0.013$ . In contrast, the same treatment of the data for PyM gives an  $r_0$  of approximately 0.4. Volumes of the equivalent spheres for PyM and Py#MPy, respectively were estimated from the

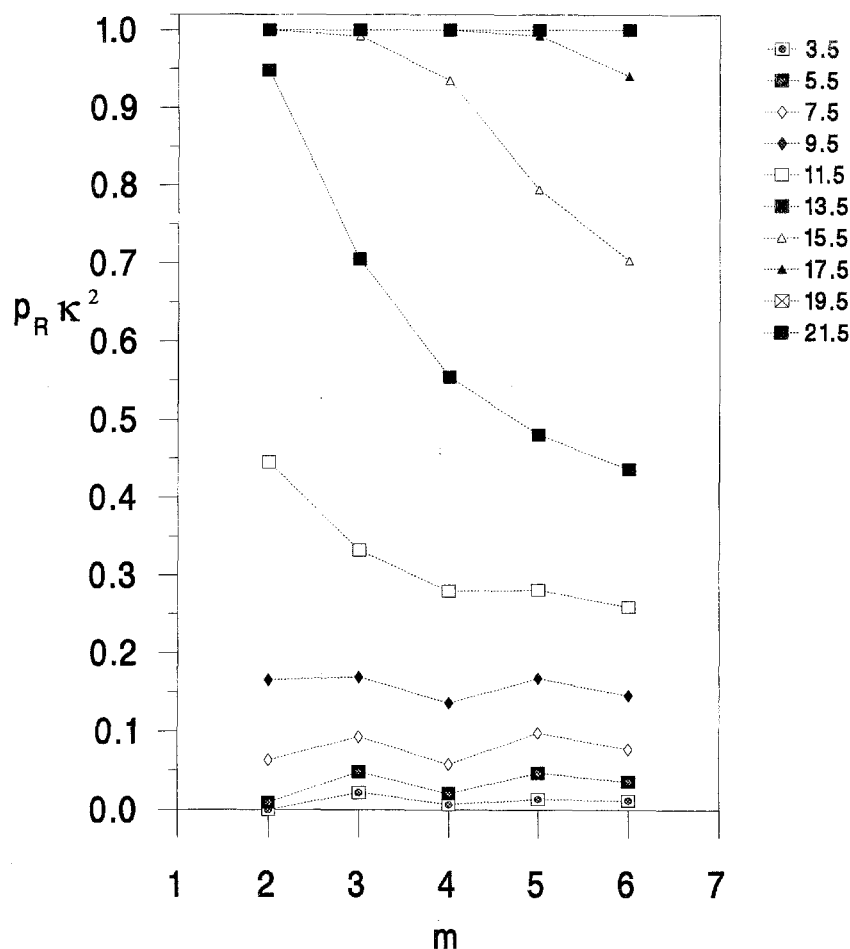


Fig. 12. Dependence of  $p_R \kappa^2$  on  $m$  for different assumed values of  $R$  in the range 3.5–21.5 Å.

slopes ( $2.3 \times 10^{-7}$  and  $3.9 \times 10^{-7}$  kg/kms<sup>2</sup>) as  $150 \pm 40$  and  $450 \pm 130$  Å<sup>3</sup>.

### Förster Radius for Self-Transfer of Energy

The ratios of the  $R_0$  for self-transfer of energy by two species ( $A^* \rightarrow A$  and  $B^* \rightarrow B$ ) under the same experimental conditions can be written as

$$\frac{R_{0,A}}{R_{0,B}} = \frac{\kappa_A^2 \phi_A J_A}{\kappa_B^2 \phi_B J_B} \quad (5)$$

where  $\kappa^2$  denotes the orientation factor,  $\phi$  denotes the quantum yield for the fluorescence of the donor, and  $J$  denotes the overlap integral for the excitation spectrum of the acceptor and the emission spectrum of the donor, normalized to one. The ester group bonded to the pyrene causes these terms to be different for the chromophores

in Py#MPy than for free pyrene, as illustrated for  $J$  in Fig. 9. This figure depicts excitation and emission spectra normalized to one for pyrene and PyM in *p*-dioxane at 25°C. The overlap integral is an order of magnitude larger for PyM  $\rightarrow$  PyM than for pyrene  $\rightarrow$  pyrene.

To estimate  $R_0$  for the self-transfer from one pyrene to the other pyrene in Py#MPy measurements of  $\phi$  and  $J$  for PyM and pyrene in four solvents (*p*-dioxane, 1,2-dichloroethane, methanol, and ethylene glycol) were performed. Quantum yields for fluorescence from pyrene and PyM as donors are at the ratios 1:9.7, 1:7.9, 1:13.4, and 1:1.8 in *p*-dioxane, 1,2-dichloroethane, methanol, and ethylene glycol, respectively, and the  $J$  for pyrene  $\rightarrow$  pyrene and PyM  $\rightarrow$  PyM are at the ratios 1:11.8, 1:12.8, 1:6.5 and 1:22.1, respectively, in the same solvents. Combining both effects, and assuming that  $R_0$  is 10.05 Å for free pyrene  $\rightarrow$  free pyrene,<sup>(15)</sup> the estimated

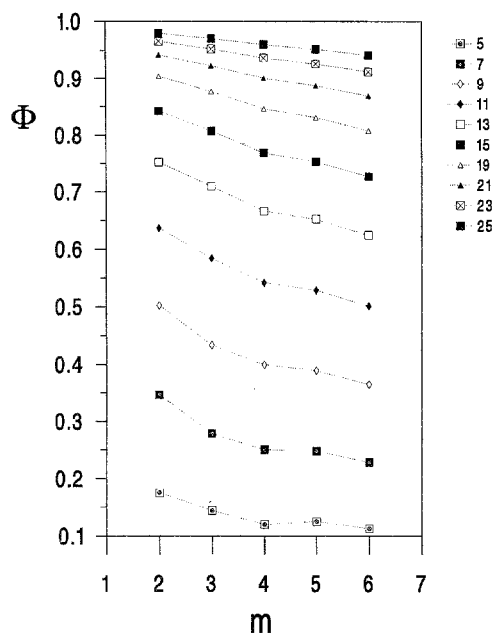


Fig. 13. Efficiency of Förster transfer,  $\Phi$ , on  $m$  for different assumed values of  $R$  in the range 5–25 Å.

values of  $R_0$  for PyM and Py-COO-(CH<sub>2</sub>)<sub>m</sub>-OOC-Py are 22.2, 21.7, 21.2, and 18.6 Å in *p*-dioxane, 1,2-dichloroethane, methanol, and ethylene glycol, respectively. The average  $\pm$  standard deviation of the  $R_0$  is 21  $\pm$  2 Å.

## THEORETICAL INTERPRETATION

The methods used in the theoretical calculation, the geometrical parameters, and the conformational energies for the first- and second-order interactions in Py#MPy are those used previously.<sup>(12)</sup> The pyrene ring system and the ester group are both planar and have a dihedral angle of about 40° between their planes. This angle is obtained in four isoenergetic conformations by appropriate rotation around the C<sub>carbonyl</sub>-C<sub>aromatic</sub> bond. Nine orientations were assigned to each of the  $m + 1$  rotatable bonds in the sequence O-(CH<sub>2</sub>)<sub>m</sub>-O, by allowing the three classic rotational isomers<sup>(22)</sup> (*trans*, *gauche*<sup>+</sup>, *gauche*<sup>-</sup>) and, also symmetric displacements of  $\pm 20^\circ$  about each of these three rotational isomers. The number of conformations evaluated for each Py#MPy was  $4^{2m+1}$ . The separation of the centers of masses of the two pyrenes and the orientation factor were obtained from the calculation.

Figure 10 depicts the distribution functions for the distances between the centers of the two pyrenes in

Py#MPy. Figure 11 depicts the distribution of the function  $w_R \kappa^2$  where  $w_R$  is the probability function for the distance between the centers of mass, the rings. Figure 12 depicts the dependence of the product  $p_R \kappa^2$  on  $m$  and  $R$ . Here  $p_R$  denotes the probability of finding the center of mass of one pyrene ring within a sphere of radius  $R$  centered at the center of mass of the other pyrene ring.

$$p_R = \int_0^R w_R dR \quad (6)$$

The average values of  $\kappa^2$  were 0.78, 0.77, 0.76, 0.74, and 0.73 for  $m$  of 2, 3, 4, 5, and 6, respectively. Figure 13 depicts the efficiency of energy transfer,  $\Phi$ , defined as<sup>(23)</sup>

$$\Phi = \sum p [1 + \kappa^2 R^6 / (2/3) R_0^6]^{-1} \quad (7)$$

According to the theoretical results depicted in Fig. 12 or 13, values of  $R$  higher than approximately 19 Å give  $p_R$  and  $p_R \kappa^2$  very close to one at  $m = 2-6$ . For values of  $R$  larger than 19 Å, no conformation of Py#MPy with  $m = 2-6$  can produce a separation of the centers of mass of the two pyrenes that is larger than  $R$ . This theoretical analysis agrees with the experimental estimate of  $R$  of  $21 \pm 2$  Å and the near-independence of  $r$  from  $m$  that is observed. The value of  $R$  for self-transfer in Py#MPy is therefore twice as large as the value for self-transfer between free molecules of underivatized pyrene.

The independence of  $\Phi$  from  $m$  in the Py#MPy studied here is different from results obtained previously for similar bichromophoric model compounds where the donor/acceptor pair is naphthalene/naphthalene<sup>(16,24)</sup> or naphthalene/anthracene.<sup>(23)</sup> In the latter two series of compounds,  $\Phi$  was observed to decrease as the size of the spacer increased. The dependence of  $\Phi$  on spacer size could be observed in these compounds because of the smaller  $R_0$ , in the range 12–16 Å.

## ACKNOWLEDGMENTS

This research was supported by DGICYT PB91-0166 (E.S. and F.M.), MEC Fellowship PR94-070 (J.B.), and National Science Foundation Grant DMR 9220369 (W.L.M.).

## REFERENCES

1. J. B. Birks and L. G. Christophorou (1963) *Spectrochim. Acta* 19, 401.

2. K. A. Zachariasse, G. Duveneck, and R. Russe (1984) *J. Am. Chem. Soc.* **106**, 1045.
3. F. C. De Schryver, P. Collart, J. Vandendriessche, R. Goedeweck, A. Swinnen, and M. Van der Auweraer (1987) *Acct. Chem. Res.* **20**, 159.
4. K. A. Zachariasse and G. Striker (1988) *Chem. Phys. Lett.* **145**, 251.
5. P. Collart, S. Toppet, and F. C. De Schryver (1987) *Macromolecules* **20**, 1266.
6. K. A. Zachariasse, G. Duveneck, W. Kühnle, P. Reynders, and G. Striker (1987) *Chem. Phys. Lett.* **133**, 390.
7. P. Reynders, H. Dreeskamp, W. Kühnle, and K. A. Zachariasse (1987) *J. Phys. Chem.* **91**, 3982.
8. P. Reynders, W. Kühnle, and K. A. Zachariasse (1990) *J. Phys. Chem.* **94**, 4073.
9. K. Zachariasse and W. Kühnle (1976) *Z. Phys. Chem. Neue Folge* **101**, 267.
10. R. Andriessen, F. C. De Schryver, N. Boens, N. Ikeda, and H. Masuhara (1989) *Macromolecules* **22**, 2166.
11. P. Reynders, W. Kühnle, and K. A. Zachariasse (1990) *J. Am. Chem. Soc.* **112**, 3929.
12. F. Mendicuti, E. Saiz, and W. L. Mattice (1993) *J. Polym. Sci. Part B Polym. Phys.* **31**, 213.
13. O. Martin, F. Mendicuti, E. Saiz, and W. L. Mattice (1995) *J. Polym. Phys. Part B Polym. Phys.* **33**, 1107.
14. J. Guillet (1985) *Polymer Photophysics and Photochemistry: An Introduction to the Study of Photoprocesses in Macromolecules*, Cambridge University Press, Cambridge, p. 119.
15. I. B. Berlman (1973) *Energy Transfer Parameters of Aromatic Compounds*, Academic Press, New York.
16. F. Mendicuti, E. Saiz, and W. L. Mattice (1992) *Polymer* **33**, 4908.
17. J. R. Lakowicz (1983) *Principles of Fluorescence Spectroscopy*, Plenum Press, New York, p. 131.
18. J. R. Lakowicz (1983) *Principles of Fluorescence Spectroscopy*, Plenum Press, New York, p. 126.
19. F. C. Perrin (1929) *Ann. Phys.* **12**, 169.
20. J. R. Lakowicz (1983) *Principles of Fluorescence Spectroscopy*, Plenum Press, New York, p. 134.
21. J. R. Lakowicz (1983) *Principles of Fluorescence Spectroscopy*, Plenum Press, New York, p. 324.
22. W. L. Mattice and U. W. Suter (1994) *Conformational Theory of Large Molecules The Rotational Isomeric State Model in Macromolecular Systems*, Wiley, New York, Chap. III.
23. J. Bravo, F. Mendicuti, E. Saiz, and W. L. Mattice (1994) *Macromol. Chem. Phys.* **195**, 3411.
24. J. Gallego, F. Mendicuti, E. Saiz, and W. L. Mattice (1993) *Polymer* **34**, 2475.